9258 *Inorg. Chem.* **2009**, *48*, 9258–9270
DOI: 10.1021/ic9011394

Inorganic Chemistry
Article

Electrochemically-Induced TCNQ/$Mn[TCNQ]_2(H_2O)_2$ (TCNQ = 7,7,8,8-Tetracyanoquinodimethane) Solid−Solid Interconversion: Two Voltammetrically Distinct Processes That Allow Selective Generation of Nanofiber or Nanorod Network Morphologies

Ayman Nafady,[†] Alan M. Bond,* and Anthony P. O'Mullane[‡]

School of Chemistry, Monash University, Clayton, Victoria 3800, Australia. [†]Permanent address: Chemistry Department, Faculty of Science, Sohag University, Sohag, Egypt 82524. [‡]Present address: School of Applied Sciences, RMIT University, GPO Box 2476 V, Melbourne, Victoria 3001, Australia.

Received June 12, 2009

Unlike the case with other divalent transition metal $M[TCNQ]_2(H_2O)_2$ (M=Fe, Co, Ni) analogues, the electrochemically induced solid−solid phase interconversion of TCNQ microcrystals (TCNQ = 7,7,8,8-tetracyanoquinodimethane) to $Mn[TCNQ]_2(H_2O)_2$ occurs via two voltammetrically distinct, time dependent processes that generate the coordination polymer in nanofiber or rod-like morphologies. Careful manipulation of the voltammetric scan rate, electrolysis time, $Mn^{2+}_{(aq)}$ concentration, and the method of electrode modification with solid TCNQ allows selective generation of either morphology. Detailed *ex situ* spectroscopic (IR, Raman), scanning electron microscopy (SEM), and X-ray powder diffraction (XRD) characterization clearly establish that differences in the electrochemically synthesized Mn-TCNQ material are confined to morphology. Generation of the nanofiber form is proposed to take place rapidly via formation and reduction of a Mn-stabilized anionic dimer intermediate, $[(Mn^{2+})(TCNQ-TCNQ)_2^{\bullet -}]$, formed as a result of radical-substrate coupling between $TCNQ^{\bullet -}$ and neutral TCNQ, accompanied by ingress of Mn^{2+} ions from the aqueous solution at the triple phase TCNQ/electrode/electrolyte boundary. In contrast, formation of the nanorod form is much slower and is postulated to arise from disproportionation of the $[(Mn^{2+})(TCNQ-TCNQ)^{\bullet -}_2]$ intermediate. Thus, identification of the time dependent pathways via the solid−solid state electrochemical approach allows the crystal size of the $Mn[TCNQ]_2(H_2O)_2$ material to be tuned and provides new mechanistic insights into the formation of different morphologies.

1. Introduction

Low dimensional molecular solids based on polymeric metal-TCNQ (TCNQ = 7,7,8,8, tetracyanoquinodimethane) structures continue to attract new research interests[1] and foster many technological applications in diverse areas such as light emitting diodes,[2] data storage devices,[3] glucose biosensors,[4] organic field-effect transistors,[5] and photovoltaic

*To whom correspondence should be addressed. E-mail: alan.bond@sci.monash.edu.au. Fax: +613-9905-4597.

(1) (a) Lv, Q.-Y.; Song, Y.-Q.; Zhan, S.-Z.; Cai, J.; He, J.-P. *J. Coord. Chem.* **2009**, *62*, 1536. (b) Flannigan, D. J.; Samartzis, P. C.; Yurtsever, A.; Zewail, A. H. *Nano Lett.* **2009**, *9*, 875. (c) Trifonov, A. A.; Gudilenkov, I. D.; Fukin, G. K.; Cherkasov, A. V.; Larionova, J. *Organometallics* **2009**, *28*, 3421. (d) Kirtley, J. R.; Mannhart, J. *Nat. Mater.* **2008**, *7*, 520. (e) Ruiz, J.; Anton, M. J.; Vivanco, M.; Mosquera, M. E. G.; Quesada, R. *Inorg. Chem.* **2008**, *47*, 5540. (f) Alberola, A.; LIusar, R.; Vicent, C.; Andres, J.; Polo, V.; Gomez-Garcia, C. J. *Inorg. Chem.* **2008**, *47*, 3661. (g) Schelter, E. J.; Morris, D. E.; Scott, B. L.; Thompson, J. D.; Kiplinger, J. L. *Inorg. Chem.* **2007**, *46*, 5528. (h) Xiao, K.; Tao, J.; Pan, Z.; Puretzky, A. A.; Ivanov, I. N.; Pennycook, S. J.; Geohegan, D. B. *Angew. Chem., Int. Ed.* **2007**, *46*, 2650. (i) Savy, J.-P.; de Caro, D.; Faulmann, C.; Valade, L.; Almeida, M.; Koike, T.; Fujiwara, H.; Sugimoto, T.; Fraxedas, J.; Ondarcuhu, T.; Pasquier, C. *New J. Chem.* **2007**, *31*, 519. (j) Sakai, M.; Nakamura, M.; Kudo, K. *Appl. Phys. Lett.* **2007**, *90*, 62101. (k) Jain, R.; Kabir, K.; Gilroy, J. B.; Mitchell, K. A. R.; Wong, K.-c.; Hicks, R. G. *Nature* **2007**, *445*, 291.

(2) (a) Khan, M. A.; Xu, W.; Khizar-ul-Haq; Bai, Y.; Wei, F.; Jiang, X. Y.; Zhang, Z. L.; Zhu, W. Q. *J. Phys D: Appl. Phys.* **2007**, *40*, 6535. (b) Okamoto, T.; Kozaki, M.; Doe, M.; Uchida, M.; Wang, G.; Okada, K. *Chem. Mater.* **2005**, *17*, 5504.

(3) (a) Ran, C.; Peng, H.; Ren, L.; Zhou, W.; Ling, Y.; Liu, Z. *J. Phys. Chem. C* **2007**, *111*, 631. (b) Muller, R.; Genoe, J.; Heremans, P. *Appl. Phys. Lett.* **2006**, *88*, 242105. (c) Peng, H.; Chen, Z.; Tong, L.; Yu, X.; Ran, C.; Liu, Z. *J. Phys. Chem. B* **2005**, *109*, 3526. (d) Yu, X.; Zhang, R.; Peng, H.; Ran, C.; Zhang, Y.; Liu, Z. *J. Phys. Chem. B* **2004**, *108*, 14800. (e) Yamaguchi, S.; Potember, R. S. *Synth. Met.* **1996**, *78*, 117.

(4) (a) Cano, M.; Luis Avila, J.; Mayen, M.; Mena, M. L.; Pingarron, J.; Rodriguez-Amaro, R. *J. Electroanal. Chem.* **2008**, *615*, 69. (b) Pauliukaite, R.; Malinauskas, A.; Zhylyak, G.; Spichiger-Keller, U. E. *Electroanalysis* **2007**, *19*, 2491. (c) Cano, M.; Palenzuela, B.; Rodriguez-Amaro, R. *Electroanalysis* **2006**, *18*, 1068. (d) Palmisano, F.; Zambonin, P. G.; Centonze, D.; Quinto, M. *Anal. Chem.* **2002**, *74*, 5913.

(5) (a) Di, C.; Yu, G.; Liu, Y.; Guo, Y.; Wu, W.; Wei, D.; Zhu, D. *Phys. Chem. Chem. Phys.* **2008**, *10*, 2302. (b) Videlot-Ackermann, C.; Ackermann, J.; Fages, F. *Synth. Met.* **2007**, *157*, 551. (c) Di, C.; Yu, G.; Liu, Y.; Xu, X.; Wei, D.; Song, Y.; Sun, Y.; Wang, Y.; Zhu, D.; Liu, J.; Liu, X.; Wu, D. *J. Am. Chem. Soc.* **2006**, *128*, 16418. (d) Menard, E.; Podzorov, V.; Hur, S. H.; Gaur, A.; Gershenson, M. E.; Rogers, J. A. *Adv. Mater.* **2004**, *16*, 2097.

Published on Web 09/11/2009

cells.[6] As a result of their intriguing structural, optical, and electrical properties, the (1:1) type CuTCNQ and AgTCNQ semiconducting solids have been the most extensively investigated metal-TCNQ systems in the past decade.[7] Recent studies with these TCNQ-based materials[8] have focused on the introduction of new synthetic approaches such as vapor deposition, spontaneous electrolysis, electrospining,[9] together with electrochemical and photochemical techniques[10] to control their intrinsic physical and chemical properties and hence improve their mechanical stability, as well as their semiconducting and switching properties.

In the case of binary (1:2) $M[TCNQ]_2$ (M = V, Mn, Fe, Co, Ni, Zn) transition metal molecular materials, only sporadic interest[11] was shown in the period immediately following their initial synthesis by Melby et al. over 40 years ago.[12] However, extensive recent studies by Dunbar and Miller have reinvigorated interest in this class of compound. Despite the successful chemical synthesis of different forms of the divalent cation (M^{2+}) transition metal family, including the solvent-free $M[TCNQ]_2$ ($M = Mn^{2+}$, Fe^{2+}, Co^{2+}, Ni^{2+}) "glassy magnets"[14] and the solvated $M[TCNQ]_2(s)_2$, (s = MeOH or H_2O)[15] congeners, their insolubility, structural complexity, and possible polymorphism often preclude the growth of large single crystals suitable for X-ray analysis. A notable exception is the elegant work of Dunbar and co-workers that has produced crystal structures of a family of Mn- and Zn-TCNQ based compounds.[13a,15] These investigations have revealed a range of binding modes for the $TCNQ^{\bullet-}$ ligand (e.g., *cis*-[μ-TCNQ]$^{\bullet-}$, *syn*-[μ-TCNQ]$^{\bullet-}$, and μ_4-[TCNQ−TCNQ]$^{2-}$) in unique network polymers having extensive supramolecular interactions between layers through hydrogen-bonding or $\pi-\pi$ stacking.[13a,15] Thus, methanol solvated polymeric structures such as $Mn[(TCNQ)_2(MeOH)_2]$, $[Mn(TCNQ-TCNQ)(MeOH)_4]_\infty$, and $[Mn(TCNQ)(TCNQ-TCNQ)_{0.5}(MeOH)_2]_\infty$ have been synthesized and characterized.[15] In contrast, only one phase and formulation, consisting of Mn(II) ions bonded to two *syn*-[μ-TCNQ$^{\bullet-}$] equatorial ligands and two axial H_2O molecules, is available as a hydrated $Mn[TCNQ]_2(H_2O)_2$ analogue, although in this case non-identical X-ray powder diffraction patterns were found for single crystals and bulk material.[15]

Given the structural versatility and richness of the Mn-TCNQ based material, and our interest in electrochemically driven $TCNQ/M[TCNQ]_2(H_2O)_2$ solid−solid phase transformation processes,[16] we have now set out to probe the mechanistic nuances associated with the electrochemical conversion of TCNQ-modified (GC, Pt, Au, or ITO) electrodes, in contact with an aqueous solution of Mn^{2+} ions, into Mn-TCNQ material. In contrast to electrochemical studies that generate other $M[TCNQ]_2(H_2O)_2$ (M = Fe, Co, Ni) compounds,[16] the solid−solid interconversion process in the manganese case takes place via two voltammetrically distinguishable, time-dependent processes that produce nanofiber and/or nanorod forms of $Mn[TCNQ]_2(H_2O)_2$. Nevertheless, X-ray diffraction, energy dispersive X-ray analysis, IR, and Raman characterization all imply the presence of only one crystalline phase, namely, the hydrated $Mn[TCNQ]_2(H_2O)_2$, in the final product.

2. Experimental Section

2.1. Materials and Chemical Synthesis of $Mn[TCNQ]_2(H_2O)_2$. All chemicals and solvents were used as received from the manufacturer. Hydrated $Mn(NO_3)_2 \cdot xH_2O$ (98%), $MnCl_2 \cdot 4H_2O$ (98%), 7,7,8,8-tetracyanoquinodimethane (TCNQ, 99%), and r*eagentplus* acetonitrile (99%) were purchased from Aldrich. $[Bu_4N][ClO_4]$ (Aldrich) was recrystallized several times from ethanol (95%) and vacuum-dried prior to use. $Mn[TCNQ]_2(H_2O)_2$ was synthesized chemically using a procedure based on that reported by Dunbar et al.[15] To an aqueous solution (5.0 mL) of $MnCl_2 \cdot 4H_2O$ (0.015 g, 0.125 mmol) a solution (5.0 mL) of LiTCNQ (0.053 g, 0.25 mmol) was added with stirring. The mixture immediately became dark blue in color and a blue precipitate appeared. The mixture was stirred for 30 min at room temperature, and the resulting blue suspension filtered over a medium porosity frit to isolate the crude product as a deep blue-purple solid. The solid was washed sequentially with water (5×10 mL), ethanol (3×5 mL), and diethyl ether until the washings were colorless, and then dried under vacuum. The isolated blue-purple solid was confirmed to be

(6) (a) Iwase, T.; Haga, Y. *J. Mater. Sci.: Mater. Electronics* **2004**, *15*, 617. (b) Fortin, D.; Drouin, M.; Harvey, P. D. *Inorg. Chem.* **2000**, *39*, 2758. (c) Harvey, P. D; Fortin, D. *Coord. Chem. Rev.* **1998**, *171*, 351.

(7) (a) Ouyang, C.; Guo, Y.; Liu, H.; Zhao, Y.; Li, G.; Li, Y.; Song, Y.; Li, Y. *J. Phys. Chem. C* **2009**, *113*, 7044. (b) Shen, H.; Zheng, K.; Li, J.; Sun, D.; Chen, G. *Nanotechnology* **2008**, *19*, 015305. (b) Flannigan, D. J.; Lobastov, V. A.; Zewail, A. H. *Angew. Chem., Int. Ed.* **2007**, *46*, 9206. (c) Xiao, K.; Ivanov, I. N.; Puretzky, A. A.; Liu, Z.; Geohegan, D. B. *Adv. Mater.* **2006**, *18*, 2184. (d) Mo, X.-L.; Chen, G.-R.; Cai, Q.-J.; Fan, Z.-Y.; Xu, H.-H.; Yao, Y.; Yang, J.; Gu, H.-H.; Hua, Z.-Y. *Thin Solid Films* **2003**, *436*, 259. (e) Jerome, D.; Schulz, H. J. *Adv. Phys.* **2002**, *51*, 293.

(8) (a) Tian, F.; Liu, W.; Wang, C.-R. *J. Phys. Chem. C* **2008**, *112*, 8763. (b) Cui, S.; Li, Y.; Guo, Y.; Liu, H.; Song, Y.; Xu, J.; Lv, J.; Zhu, M.; Zhu, D. *Adv. Mater.* **2008**, *20*, 309. (c) Billen, J.; Steudel, S.; Muller, R.; Genoe, J.; Heremans, P. *Appl. Phys. Lett.* **2008**, *91*, 263507. (d) Zhou, X.-H.; Wei, S.-J.; Zhang, S.-S. *Langmuir* **2008**, *24*, 4464. (e) Liu, Y.; Li, H.; Ji, Z.; Kashimura, Y.; Tang, Q.; Furukawa, K.; Torimitsu, K.; Hu, W.; Zhu, D. *Micron* **2007**, *38*, 536.

(9) (a) Matsushima, T.; Adachi, C. *Thin Solid Films* **2008**, *517*, 874. (b) Xiao, K.; Tao, J.; Puretzky, A. A.; Ivanov, I. N.; Retterer, S. T.; Pennycook, S. J.; Geohegan, D. B. *Adv Funct. Mater.* **2008**, *18*, 3043. (c) Kever, T.; Nauenheim, C.; Boettger, U.; Waser, R. *Thin Solid Films* **2006**, *515*, 1893. (d) Liu, Y.; Li, H.; Tu, D.; Ji, Z.; Wang, C.; Tang, Q.; Liu, M.; Hu, W.; Liu, Y.; Zhu, D. *J. Am. Chem. Soc.* **2006**, *128*, 12917. (e) Shang, T.; Yang, F.; Zheng, W.; Wang, C. *Small* **2006**, *2*, 1007. (f) Cao, G.; Ye, C.; Fang, F.; Xing, X.; Xu, H.; Sun, D.; Chen, G. *Micron* **2005**, *36*, 267.

(10) (a) Zhao, C.; Bond, A. M. *J. Am. Chem. Soc.* **2009**, *131*, 4279. (b) Nafady, A.; Bond, A. M.; Bilyk, A.; Harris, A. R.; Bhatt, A. I.; O'Mullane, A. P.; De Marco, R. *J. Am. Chem. Soc.* **2007**, *129*, 2369. (c) O'Mullane, A. P.; Fay, N; Nafady, A.; Bond, A. M. *J. Am. Chem. Soc.* **2007**, *129*, 2066. (d) Harris, A. R.; Nafady, A.; O'Mullane, A. P.; Bond, A. M. *Chem. Mater.* **2007**, *19*, 5499. (e) Harris, A. R.; Neufeld, A. K.; O'Mullane, A. P.; Bond, A. M. *J. Mater. Chem.* **2006**, *16*, 4397. (f) Harris, A. R.; Neufeld, A. K.; O'Mullane, A. P.; Bond, A. M.; Morrison, R. J. S. *J. Electrochem. Soc.* **2005**, *152*, C577. (g) Neufeld, A. K.; O'Mullane, A. P.; Bond, A. M. *J. Am. Chem. Soc.* **2005**, *127*, 13846.

(11) (a) Siedle, A. R.; Candela, G. A.; Finnegan, T. F. *Inorg. Chim. Acta* **1979**, *35*, 125. (b) Kathirgamanathan, P.; Rosseinsky, D. R. *J. Chem. Soc., Chem. Commun.* **1980**, 839. (c) Long, G.; Willett, R. D. *Inorg. Chim. Acta* **2001**, *313*, 1.

(12) Melby, L. R.; Harder, R. J.; Hertler, W. R.; Mahler, W.; Benson, R. E.; Mochel, W. E. *J. Am. Chem. Soc.* **1962**, *84*, 3374.

(13) (a) Zhao, H.; Heintz, R. A.; Dunbar, K. R.; Rogers, R. D. *J. Am. Chem. Soc.* **1996**, *118*, 12844. (b) Zhao, H.; Heintz, R. A.; Ouyang, X.; Grandinetti, G.; Cowen, J.; Dunbar, K. R. *NATO ASI Ser. Ser. C* **1999**, *518*, 353. (c) Pokhodnya, K. I.; Petersen, N.; Miller, J. S. *Inorg. Chem.* **2002**, *41*, 1996. (d) Vickers, E. B.; Selby, T. D.; Thorum, M. S.; Taliaferro, M. L.; Miller, J. S. *Inorg. Chem.* **2004**, *43*, 6414. (e) Lopez, N.; Zhao, H.; Prosvirin, A. V.; Chouai, A.; Shatruk, M.; Dunbar, K. R. *Chem. Commun.* **2007**, *44*, 4611. (f) Motokawa, N.; Miyasaka, H.; Yamashita, M.; Dunbar, K. R. *Angew. Chem., Int. Ed.* **2008**, *47*, 7760.

(14) (a) Clerac, R.; O'Kane, S.; Cowen, J.; Ouyang, X.; Heintz, R.; Zhao, H.; Bazile, M. J., Jr.; Dunbar, K. R. *Chem. Mater.* **2003**, *15*, 1840. (b) Vickers, E. B.; Giles, I. D.; Miller, J. S. *Chem. Mater.* **2005**, *17*, 1667.

(15) Zhao, H.; Heintz, R. A.; Ouyang, X.; Dunbar, K. R.; Campana, C. F.; Rogers, R. D. *Chem. Mater.* **1999**, *11*, 736.

(16) (a) Nafady, A.; Bond, A. M.; Bilyk, A. *J. Phys. Chem. C* **2008**, *112*, 6700. (b) Nafady, A.; Bond, A. M. *Inorg. Chem.* **2007**, *46*, 4128. (c) Nafady, A.; O'Mullane, A. P.; Bond, A. M.; Neufeld, A. K. *Chem. Mater.* **2006**, *18*, 4375.

hydrated $Mn[TCNQ]_2(H_2O)_2$ via comparison of IR and XRD data with that reported in the literature.[15]

2.2. Electrochemical Procedures. A fresh aqueous solution of Mn^{2+} electrolyte was prepared daily and kept in the dark under N_2 to avoid air-oxidation and formation of solid MnO_2. Aqueous electrolyte solutions were prepared using water purified by a Millipore System (resistivity of 18.2 MΩ cm). Voltammetric measurements were undertaken with an Autolab PGSTAT100 (ECO-Chemie) workstation using a standard three-electrode cell configuration. The working electrodes used were glassy carbon (GC) disk (3 mm diameter) platinum (Pt) and gold (Au) (1.6 mm diameter) obtained from Bioanalytical Systems as well as semiconducting indium tin oxide (ITO)-coated glass (0.02−0.1 cm^2 area) having a 10 Ω/sq sheet resistance (as quoted by the manufacturer Prazisions Glas and Optik GmbH). These electrodes were routinely cleaned and polished according to the procedures described in reference 16. TCNQ-modified versions of these working electrodes (GC, Pt, Au, and ITO) were prepared via drop casting or mechanical attachment as described elsewhere.[16c] The auxiliary electrode consisted of large surface area platinum mesh, and the reference electrode was an aqueous Ag/AgCl (3.0 M KCl) from Bioanalytical Systems, against which all potentials are reported at 23 ± 2 °C.

2.3. Physical Measurements. Details related to infrared spectroscopy (IR), Powder X-ray diffraction (XRD), scanning electron microscopy (SEM), and energy-dispersive X-ray (EDX) instruments and measurements are described elsewhere.[16c] Raman spectra were recorded by using a Renishaw RM 2000 Raman spectrograph and microscope with 50× objective lens. Because of the sensitivity of the Mn-TCNQ based material to laser light, only 1−10% of the laser strength (18 mW) was used at a wavelength of 780 nm. Nevertheless, microscopic examination of Mn-TCNQ solid samples after exposure to the laser light for only 30 s revealed a color change from blue to purple for the irradiated spot.

3. Results

3.1. Electrochemical Investigations of the TCNQ/Mn-TCNQ Solid−Solid Interconversion. 3.1.1. Voltammetric Studies of Solid TCNQ in Contact with $Mn^{2+}{}_{(aq)}$ Electrolyte. Cyclic voltammograms obtained at a scan rate of 20 mV s^{-1} over the potential range of 0.35 to −0.10 V versus Ag/AgCl with bare or TCNQ-modified GC electrodes (via drop casting or mechanical attachment methods) in the presence of 0.10 M $Mn(NO_3)_{2(aq)}$ electrolyte are presented in Figure 1. Evidently, $Mn^{2+}{}_{(aq)}$ ions are electrochemically inactive over the designated potential range when a bare GC electrode is used (Figure 1a). Thus, the observed electrochemical activity of TCNQ-modified electrodes via drop casting (Figure 1b) or mechanical attachment (Figure 1c) is attributed to the one-electron reduction of TCNQ into $TCNQ^{\bullet-}$ and its concomitant transformation into Mn-TCNQ based material upon ingress of Mn(II) ions.

As noted with other $TCNQ/M[TCNQ]_2(H_2O)_2$ (M = Fe^{2+}, Co^{2+}, Ni^{2+}) interconversions,[16] less complicated and more reproducible cyclic voltammograms were obtained, in the initial cycles of potential, when the mechanical attachment method is used compared to the drop casting method (Figure 1 panel b vs c). This is likely to be associated with the ingress/egress of $Mn^{2+}{}_{(aq)}$ ions into/from the $TCNQ^{\bullet-}$ crystal lattice channels being able to take place more rapidly with the smaller TCNQ microparticles obtained via mechanical attachment than with much larger TCNQ crystals produced by the drop casting

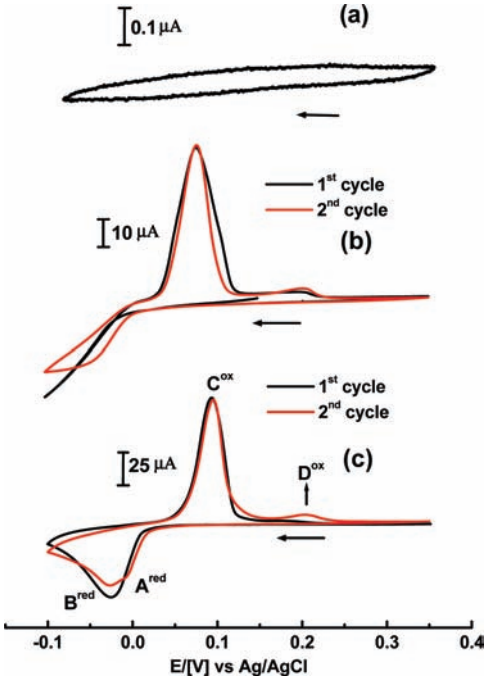

Figure 1. Cyclic voltammograms in the presence of 0.10 M $Mn(NO_3)_{2(aq)}$ electrolyte obtained at a scan rate of 20 mV s^{-1} with (a) a bare 3.0 mm diameter GC electrode, (b) GC electrode modified with solid TCNQ via the drop cast method, and (c) GC electrode modified with TCNQ via the mechanical attachment method when the of the potential was cycled over the range of 0.35 to −0.10 V.

method.[16c] However, the voltammetry exhibits intriguing features not exhibited by the $TCNQ/M[TCNQ]_2(H_2O)_2$ (M = Fe^{2+}, Co^{2+}, Ni^{2+}) systems.[16] Thus, in the manganese case, even under the most optimized conditions, the reduction component displays a much broader process (peak width at half-height, $W_{1/2}{}^{red} \sim 60-70$ mV compared to 32−40 mV for the cobalt analogue)[16c] in the first cycle of potential. Furthermore, in second and subsequent cycles resolution into two closely spaced processes, labeled A^{red} and B^{red} in Figure 1c, is observed. On reversing the scan direction, a narrow ($W_{1/2}{}^{ox} \sim$ 28−35 mV) and intense oxidation process (C^{ox}) is detected at $E_p{}^{ox} \approx 90$ mV, which is followed by a second relatively minor oxidation process, labeled as (D^{ox}), at more positive potentials ($E_p{}^{ox} \approx 200$ mV).

Although the basic voltammetric behavior is essentially independent of electrode material (Pt, Au, GC, and ITO) and Mn^{2+} counteranion (e.g., ClO_4^-, Cl^-, or NO_3^-), as found in the $TCNQ/M[TCNQ]_2(H_2O)_2$ (M = Fe, Co, Ni) transformation processes,[16] the redox processes, in the manganese case, are highly influenced by scan rate, electrolysis time, and the number of cycles of potential. Figure 2 illustrates the scan rate (ν) dependence of the TCNQ/Mn-TCNQ transformation processes when a TCNQ-modified GC electrode is placed in contact with a 0.10 M $Mn^{2+}{}_{(aq)}$ solution. At very slow scan rates (1 mV s^{-1}, Figure 2a) the voltammetric response is much simpler than when using a scan rate of 20 mV s^{-1}, as in Figure 1 and indeed very similar to those obtained for the analogous $TCNQ/M[TCNQ]_2(H_2O)_2$ (M = Fe, Co, Ni) solid−solid interconversions.[16] Thus, as seen in Figure 2a, only one sharp reduction process labeled as F^{red} is obtained ($E_p{}^{red} \approx 0$ mV, $W_{1/2}{}^{red} \approx 40$ mV) in the negative potential scan direction. On

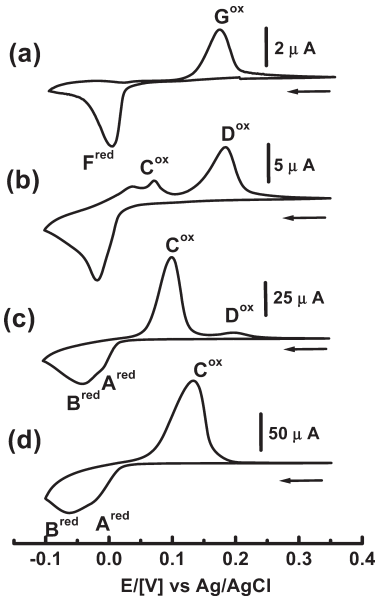

Figure 2. Cyclic voltammograms (2nd cycle of potential shown) obtained at different scan rates: (a) 1 mV s^{-1}, (b) 5 mV s^{-1}, (c) 30 mV s^{-1} and (d) 100 mV s^{-1}, when a TCNQ-modified GC electrode (mechanical attachment method) is immersed in 0.10 M $Mn(NO_3)_{2(aq)}$ electrolyte solution.

the reverse positive potential direction scan, only one oxidation counterpart (G^{ox}) is seen at $E_p^{ox} \approx 180$ mV with $W_{1/2}{}^{ox} \approx 45$ mV. The "inert zone" ($\Delta E_p = E_p^{ox} - E_p^{red}$) between processes F^{red} and G^{ox} at slow scan rate is now 180 mV, and the voltammetry has the characteristics of an electrochemically irreversible solid−solid conversion governed by nucleation−growth kinetics.[17]

ΔE_p values of 250, 225, and 153 mV have been reported for separation of reduction and oxidation components of other TCNQ/M[TCNQ]$_2$(H$_2$O)$_2$ transformations (M = Fe^{2+}, Co^{2+}, Ni^{2+}, respectively),[16] thereby indicating that the identity of the transition metal cation plays a significant role in the kinetics of these redox-induced, nucleation−growth based transformations. Importantly, despite the large value of ΔE_p (180 mV) found in the Mn-TCNQ case, and hence substantial electrochemical irreversibility of couple F^{red} and G^{ox}, the magnitude of the charge (Q) associated with the reduction component (Figure 2a) $Q(F^{red}) = 263 \pm 5\ \mu C$ is equal to that of the corresponding oxidation component $Q(G^{ox}) = 260 \pm 5\ \mu C$ within experimental error. It is therefore concluded that F^{red}/G^{ox} couple is chemically reversible under slow scan rate conditions, which implies that the Mn-TCNQ based material generated via process F^{red} can be quantitatively converted back to solid TCNQ and $Mn^{2+}{}_{(aq)}$ ions upon oxidation through process G^{ox}.

As the scan rate is increased from 1 to 5 and then 30 mV s^{-1} (Figure 2a,b,c) the reduction process (F^{red}) splits into two processes labeled in Figure 1 as A^{red} and B^{red} with the latter process, B^{red}, being more evident at higher scan rates. Furthermore, on the positive potential scan direction, two well separated oxidation processes C^{ox} and D^{ox}

(17) (a) Suarez, M. F.; Marken, F.; Compton, R. G.; Bond, A. M.; Miao, W.; Raston, C. L. *J. Phys. Chem. B* **1999**, *103*, 5637. (b) Bond, A. M.; Fletcher, S.; Symons, P. G. *Analyst* **1998**, *123*, 1891. (c) Wooster, T. J.; Bond, A. M. *Analyst* **2003**, *128*, 1386.

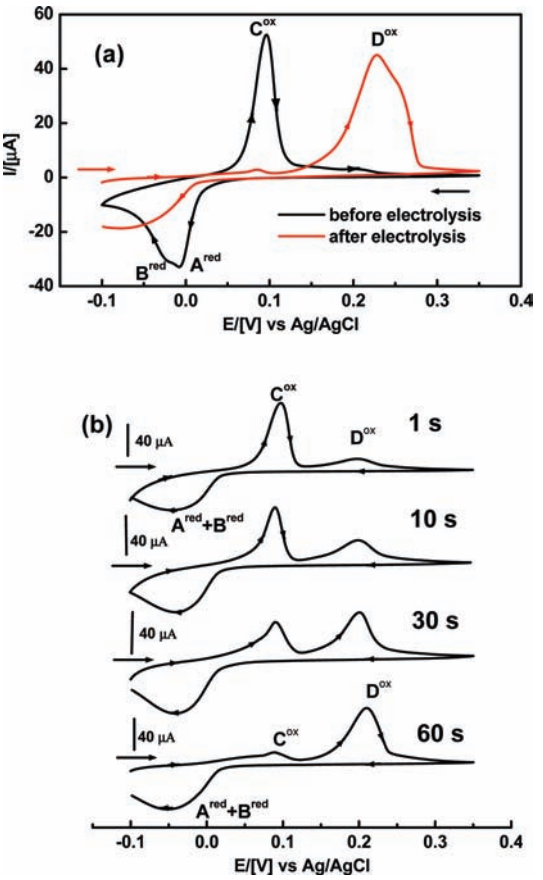

Figure 3. Cyclic voltammograms obtained at scan rate of 20 mV s^{-1} (a) before (black curve) and after 10 min of reductive electrolysis ($E_{appl} = -0.10$ V) (red curve) of a TCNQ-modified GC electrode (mechanical attachment method) in contact with 0.10 M $Mn(NO_3)_{2(aq)}$ solution (b) as in (a), but as a function of electrolysis time.

($D^{ox} \cong G^{ox}$) are observed, with process C^{ox} increasing at the expense of D^{ox}, upon increasing the scan rate. Interestingly, at even faster scan rates ($\nu \geq 100$ mV s^{-1}, Figure 2d), only one broad oxidation peak (C^{ox}) is detected in spite of the presence of the two reduction processes (A^{red}, B^{red}). This means that at fast scan rates, reduction processes A^{red} and B^{red}, in combination, lead to generation of a Mn-TCNQ based product that can be oxidized only via process C^{ox}.

The scan rate dependence clearly signals the time-dependent nature of the redox chemistry associated with the TCNQ/Mn-TCNQ solid−solid transformation. The same conclusion also is reached via careful manipulation of time under reductive electrolysis conditions, prior to implementing potential cycling. Thus, as illustrated in Figure 3a, the cyclic voltammogram (black curve) obtained under conditions of Figure 1c when the potential is initially scanned in the negative direction from 0.35 to −0.10 V then back to 0.35 V at a rate of 20 mV s^{-1}, shows the predominance of process C^{ox} relative to D^{ox}. However, if 10 min of reductive electrolysis of TCNQ-modified GC electrode at $E_{appl} = -0.10$ V is undertaken prior to commencing cyclic voltammetry, the positive going potential scan shows almost exclusive dominance (97%) of process D^{ox} ($E_p{}^{ox} = 0.23$ V). Thus, as is the case when slow scan rates are employed in cyclic voltammetry, long time scale bulk electrolysis experiments favor process

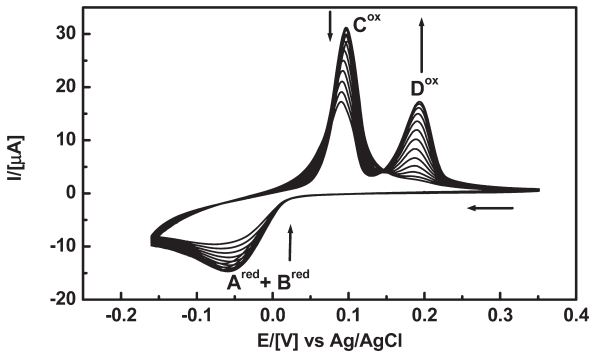

Figure 4. Cyclic voltammograms (first 13 cycles of potential) obtained at a scan rate of 20 mV s^{-1} when a TCNQ-modified GC electrode prepared via the mechanical attachment method is placed in contact with 0.10 M $Mn(NO_3)_{2(aq)}$ electrolyte and scanned over the potential range of 0.35 to −0.15 V.

D^{ox}. Detailed examination of the dependence of the two oxidation processes on electrolysis time (1 to 60 s) (Figure 3b) reveals that both processes C^{ox} and D^{ox} are detectable at very short (1 s) electrolysis times (Figure 3b top), but, as expected, process C^{ox} is the dominant one. As the electrolysis time is increased, the voltammograms progressively exhibit a marked increase in the ratio of process D^{ox} to C^{ox}, with almost exclusive dominance (95%) of the former being achieved at 60 s (Figure 3b bottom curve). Taken together, the voltammetric and bulk electrolysis data indicate that when TCNQ microcrystals are reduced in the presence of $Mn^{2+}{}_{(aq)}$ electrolyte, Mn-TCNQ based material is produced via two voltammetrically distinct, time-dependent processes (A^{red}, B^{red}).

A critical and unique finding, pertinent only to the Mn-system and not the analogous $M[TCNQ]_2(H_2O)_2$ (M = Fe^{2+}, Co^{2+}, Ni^{2+}) systems,[16] is that upon repetitive cycling of the potential over the range of 0.35 to −0.10 V, (see Figure 4 and Supporting Information, Figure S1) a gradual decrease in the peak current of the initially detected oxidation process (C^{ox}) occurs concomitantly with the emergence and progressive increase in the second more positive oxidation process (D^{ox}). The continuous increase of process (D^{ox}) at the expense of (C^{ox}) upon extended cycling of the potential (13 cycles), gives rise to the equivalent of an isosbestic point found upon monitoring the course of chemical reactions by spectroscopic methods. The long-term behavior exhibited upon this level of potential cycling may imply a slow transformation of one form of electrochemically generated Mn-TCNQ based material into another phase or polymorph. Upon very extensive cycling of potential (20−50 cycles) both processes C^{ox} and D^{ox} become gradually attenuated because of the slow dissolution of solid TCNQ[18] and/or the electrochemically generated Mn-TCNQ based material in aqueous media, as found with other members of the $M[TCNQ]_2(H_2O)_2$ family (M = Fe^{2+}, Co^{2+}, Ni^{2+}).[16]

(18) Bond, A. M.; Zhang, J. *J. Electroanal. Chem.* **2005**, *574*, 299.

(19) (a) Qu, X.; Nafady, A.; Mechler, A.; Zhang, J.; Harris, A. R.; O'Mullane, A. P.; Martin, L. L.; Bond, A. M. *J. Solid State Electrochem.* **2008**, *12*, 739. (b) O'Mullane, A. P.; Neufeld, A. K.; Bond, A. M. *Anal. Chem.* **2005**, *77*, 5447. (c) Neufeld, A. K.; Madsen, I.; Bond, A. M.; Hogan, C. F. *Chem. Mater.* **2003**, *15*, 3573.

In the CuTCNQ system,[19] related voltammetric behavior to that shown in Figure 4 is detected upon extensive cycling of the potential. In that case, the cyclic dependence is attributed to a phase change in which the initially formed, kinetically favored, highly conducting CuTCNQ phase I (σ = 0.2 S cm^{-1}) is subsequently transformed into the thermodynamically favored, relatively poorly conducting phase II material ($\sigma = 10^{-5}$ S cm^{-1}).[19b] However, careful comparison of the voltammetric behavior of the manganese and copper-TCNQ systems reveals crucial differences. First, the initial transition from phase I to phase II in the CuTCNQ case is only detected after prolonged (≥10) cycling of potential,[19c] whereas in the Mn-TCNQ system, both processes (C^{ox} and D^{ox}) are evident in the second cycle. Second, complete conversion of CuTCNQ phase I to phase II occurs after 50 cycles, but the two oxidation processes in the Mn-TCNQ remain present even after extensive cycling of potential (up to 50 cycles), implying that the time dependence and the nature of the transformations are different in the two cases. Finally, the potential separation between the two oxidation peaks [$\Delta E_p{}^{ox} = E_p(D^{ox}) - E_p(C^{ox})$] of the Mn-TCNQ system (97 mV) is significantly larger than the value ($\Delta E_p{}^{ox}$ = 32 mV)[19c] obtained for transformation of CuTCNQ phase I into phase II. Nevertheless, the tentative conclusion drawn from all the aforementioned voltammetric data is that the redox-based transformation of TCNQ microcrystals into Mn-TCNQ based material occurs through two voltammetrically distinguishable processes that give rise to two forms of Mn-TCNQ based material (not necessarily two phases).

3.1.2. Solid-State Electrochemistry of Chemically and Electrochemically Synthesized $Mn[TCNQ]_2(H_2O)_2$. Supporting Information, Figure S2 shows the cyclic voltammetric behavior obtained from electrocrystallization of Mn-TCNQ material (identified later as $Mn[TCNQ]_2(H_2O)_2$) onto a 3.0 mm diameter GC electrode via reductive electrolysis at E_{appl} = −0.15 V for 5 min in acetonitrile (0.10 M $[Bu_4N][ClO_4]$) from a solution containing 5.0 mM TCNQ and 2.50 mM $Mn(NO_3)_2$, (2:1 ratio), but under conditions where this $Mn[TCNQ]_2(H_2O)_2$-GC modified electrode is removed from the acetonitrile environment and placed in contact with 0.10 M aqueous $Mn(NO_3)_2$ electrolyte. In this experiment, the initial potential was set at −0.10 V (open circuit potential), then initially scanned in the positive potential direction to 0.40 V at a scan rate of 20 mV s^{-1}. Use of this protocol led to the observation of an intense oxidation peak at $E_p{}^{ox}$ = 0.225 V preceded by a very minor one at less positive potential ($E_p{}^{ox}$ = 0.130 V) (see red curve in Supporting Information, Figure S2). Interestingly, cycling of potential over the range of −0.10 to 0.40 V produced voltammetric features similar to those observed from TCNQ-modified electrodes in contact with 0.10 $Mn^{2+}{}_{(aq)}$ ions. Thus, initially in both cases, detection of an oxidation process similar to C^{ox} is found (blue curves in Supporting Information, Figure S2) at $E_p{}^{ox}$ = 0.155 V with the emergence and gradual increase in intensity of process D^{ox} ($E_p{}^{ox}$ = 0.225 V) being detected at the expense of C^{ox} upon extensive cycling of the potential.

Closely related behavior to that found with electrocrystallized $Mn[TCNQ]_2(H_2O)_2$ was noted when chemically

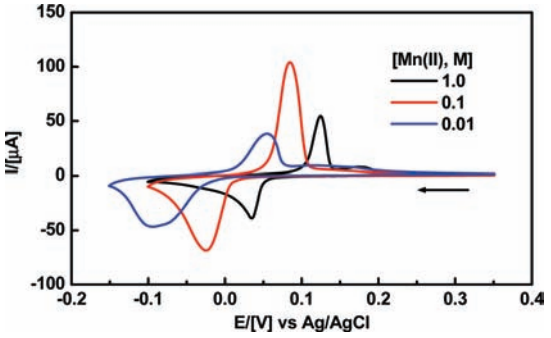

Figure 5. Cyclic voltammograms obtained without iR_u compensation at a scan rate of 20 mV s^{-1} using a TCNQ-modified GC electrode (mechanical attachment method) immersed in aqueous $Mn(NO_3)_2$ electrolyte at designated concentrations.

Table 1. Voltammetric Parameters[a] Obtained at a Scan Rate of 20 mV s^{-1} for TCNQ-Modified GC Electrodes (Mechanical Attachment Method) in the Presence of Different Concentrations of $Mn(NO_3)_{2\,(aq)}$ Solution[b]

$[Mn^{2+}{}_{(aq)}]$ (M)	E_p^{red} (V)	$W_{1/2}{}^{red}$ (mV)	E_p^{ox} (V)	$W_{1/2}{}^{ox}$ (mV)	E_m (V)	ΔE_p (mV)
0.01	−0.095	76	0.055	40	−0.020	150
0.1	−0.025	51	0.085	28	0.030	110
1	0.035	34	0.125	20	0.080	90

[a] E_p^{red} and E_p^{ox} are the reduction and oxidation peak potentials. E_m represents the midpoint potentials measured as $(E_p^{red} + E_p^{ox})/2$ in volt versus Ag/AgCl (3 M KCl); ΔE_p is the peak potential separation calculated as $(E_p^{ox} - E_p^{red})$. $W_{1/2}{}^{red}$ and $W_{1/2}{}^{ox}$ are the peak widths at half height for the reduction and oxidation processes, respectively. [b] Voltammetric data were collected after one cycle of the potential.

synthesized $Mn[TCNQ]_2(H_2O)_2$ material was mechanically attached to a GC electrode and this form of modified electrode was subjected to the same voltammetric conditions. However, in this case a more significant contribution from process (D^{ox}) was evident, even in the initial scan in the positive direction.

The multicyclic voltammetric behavior observed with electrocrystallized and chemically synthesized $Mn[TCNQ]_2(H_2O)_2$ modified electrodes implies that processes D^{ox} and C^{ox} detected in the solid−solid interconversion of TCNQ-modified electrodes immersed in $Mn^{2+}{}_{(aq)}$ electrolytes are derived from two forms of $Mn[TCNQ]_2(H_2O)_2$. Thus, oxidation of authentic samples of $Mn[TCNQ]_2(H_2O)_2$, attached to GC electrodes, initially generates solid TCNQ on the electrode surface, when the potential is initially scanned in the positive direction for the first cycle. Upon scanning in the negative direction this electrogenerated TCNQ undergoes intercalation of $Mn^{2+}{}_{(aq)}$ ions from bulk solution into the reduced $TCNQ^{\bullet-}$ lattice as is the case when commencing with pristine TCNQ-modified electrodes. Thus, the long-term behavior achieved upon repetitive cycling of the potential is independent of whether the starting point refers to a TCNQ or $Mn[TCNQ]_2(H_2O)_2$ modified electrode.

3.1.3. Effect of $Mn^{2+}{}_{(aq)}$ Concentration. Figure 5 contains cyclic voltammograms obtained at a scan rate of 20 mV s^{-1} for the TCNQ/Mn-TCNQ interconversion as a function of $Mn^{2+}{}_{(aq)}$ electrolyte concentration (0.01 to 1.0 M). Apparently, the $Mn^{2+}{}_{(aq)}$ concentration has little effect on the interplay of the redox chemistry, but the

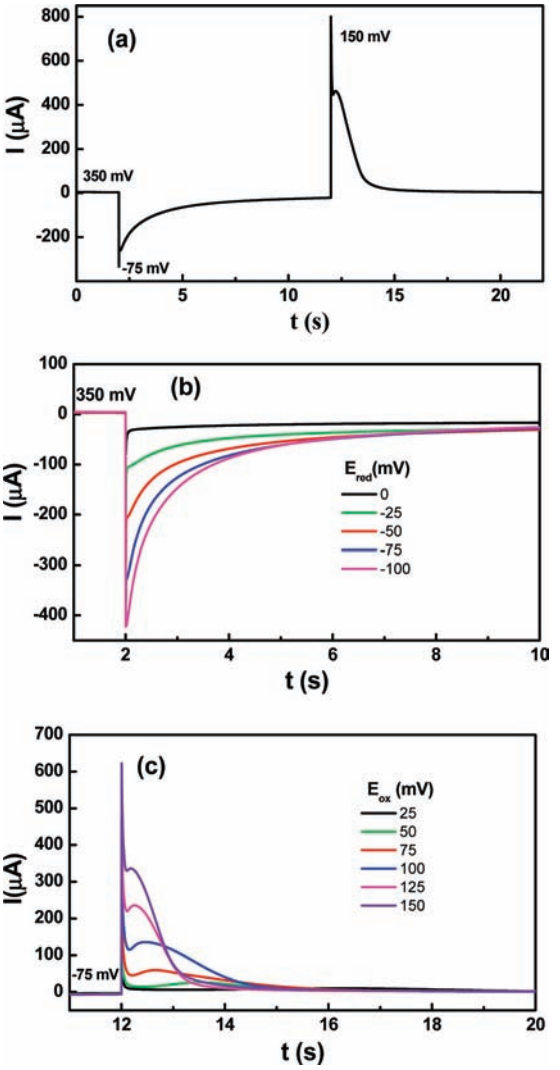

Figure 6. Double-potential step chronoamperograms obtained when a GC electrode modified with microcrystals of TCNQ (mechanical attachment) is placed in contact with 0.1 M $Mn(NO_3)_{2(aq)}$: (a) *I-t* curve obtained when the potential is stepped from $E_i = 350$ to $E_{red} = -75$ mV to induce reduction and then back to $E_{ox} = 150$ mV to induce oxidation. (b) *I-t* curves obtained under same condition as in (a), when the potential is progressively stepped from $E_i = 350$ mV to designated E_{red} potentials to induce reduction. (c) *I-t* profiles obtained when the potential is stepped from −75 mV to induce reduction then stepped back to designated E_{ox} potentials to induce oxidation. These data are collected after 2 cycles of the potential ($\nu = 100$ mV s^{-1}) and were undertaken over the range from 350 to −100 mV.

peak potentials shift significantly toward more positive values (see Table 1) upon increasing the $Mn^{2+}{}_{(aq)}$ ion concentration from 0.01 to 1.0 M. The peak-to-peak separations (ΔE_p) exhibit significant increases upon decreasing the $Mn^{2+}{}_{(aq)}$ concentration from 1.0 to 0.01 M (Table 1), although it should be noted that ΔE_p values, particularly at low electrolyte concentrations (0.01 M), are expected to be drastically influenced by uncompensated ohmic iR_u drop.[16]

3.1.4. Evidence for Nucleation−Growth Kinetics in the TCNQ/Mn-TCNQ Solid−Solid Interconversions. (a). Cyclic Voltammetry. It is generally understood that the detection of current loops in cyclic voltammograms at the onset of either the reduction or the oxidation, when the scan direction is reversed at the foot of a process, is diagnostic of rate-determining nucleation

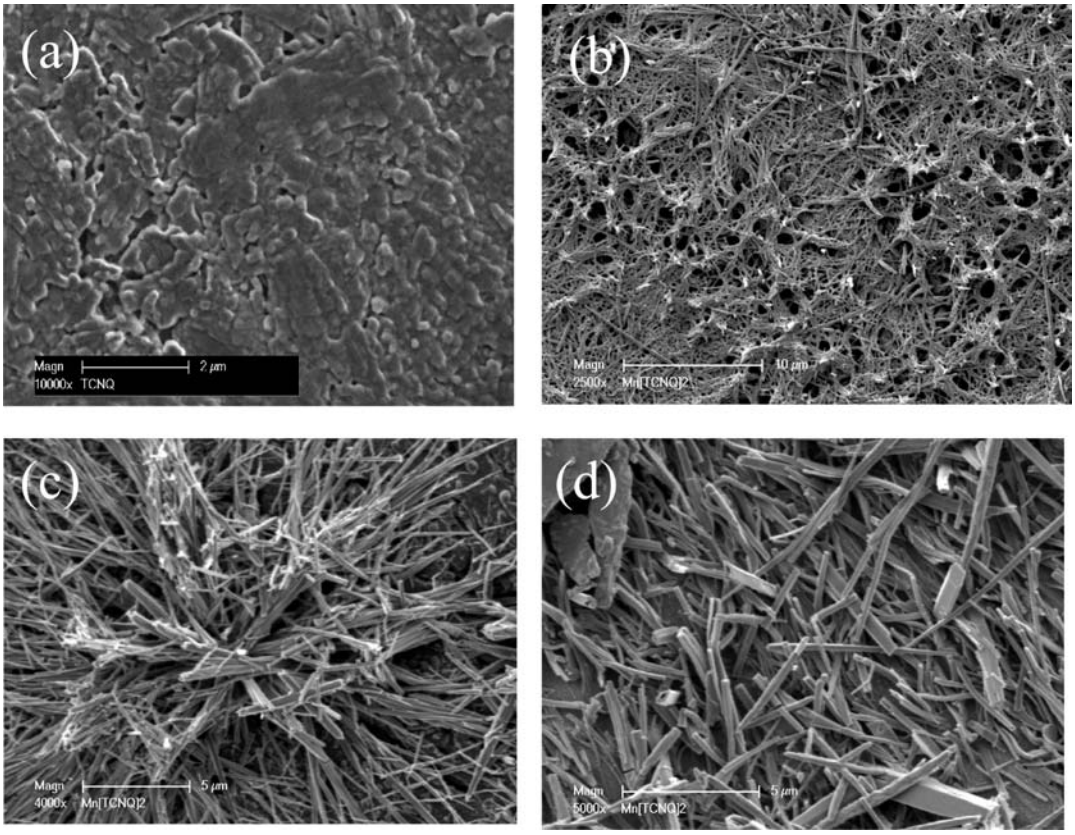

Figure 7. (a) SEM image of a TCNQ-modified ITO electrode prepared via mechanical attachment method. Images (b, c) reveal the morphology (at different magnifications) of the electrochemically generated Mn-TCNQ material obtained after completion of 2.5 cycles of potential at a scan rate of 100 mV s^{-1} over the range of 0.35 to −0.10 V using a TCNQ-modified ITO electrode (morphology initially as in image (a)) in contact with 0.10 M $Mn(NO_3)_{2(aq)}$ electrolyte. Image (d) depicts the morphology of Mn-TCNQ solid formed under conditions for (b) except that a lower scan rate (ν = 1 mV s^{-1}) was used.

and growth kinetics.[20] Observation of this phenomenon is well documented in the electrochemically induced transformation of solid TCNQ into the congeners $M[TCNQ]_2(H_2O)_2$ (M = Fe, Co, Ni)[16] as well as CuTCNQ[19c] and group I cations.[17c] However, the detection of current loops in the mechanistically more complex manganese case is only seen under special conditions. Thus, in the TCNQ/Mn-TCNQ transformation processes, the current loops found in the other systems are not observed in the initial cycles of potential upon switching the potential at the foot of the reduction process (0 V).

(b). Chronoamperometry. Definitive evidence for the presence of nucleation−growth rate-determining kinetics is obtained by performing double potential step chronoamperometric (DPSCA) experiments.[16,21] Figure 6a illustrates the current−time (*I-t*) transient obtained by stepping the potential from an initial value (E_i = 350 mV), where no redox activity is involved, to a more negative value (E_{red} = −75 mV) to induce the reduction of TCNQ for 10 s after which the potential is stepped back (oxidation direction) to E_{ox} of 150 mV, which is more positive than process C^{ox}, but not enough to initiate oxidation process D^{ox}. This potential step protocol along with conditions provided in the caption to Figure 6 allowed for observation of current−time profiles involving rapid decay in current followed by an increase to give a current maximum followed again by current decay that is diagnostic for the existence of nucleation−growth.[16,21]

3.2. SEM Examination of the Morphology Changes Accompanying the Redox-Based TCNQ/Mn-TCNQ Solid−Solid Interconversion. Figure 7 provides SEM images of TCNQ and Mn-TCNQ material, obtained from mechanical attachment of solid TCNQ onto ITO surfaces, before (image a) and after (images b−d) being in contact with 0.10 M $Mn^{2+}{}_{(aq)}$ electrolyte under cyclic voltammetric conditions (2.5 cycles of the potential over the range from 0.35 to −0.10 V). Clearly, the morphology of electrochemically generated Mn-TCNQ material (Figure 7b) differs drastically from that of initially present form of TCNQ microparticles (Figure 7a). When fast scan rate ($\nu \geq$ 100 mV s^{-1}) conditions are used to induce the TCNQ/Mn-TCNQ transformation, a relatively uniform nanofibrous network (Figure 7b) of presumably Mn-TCNQ crystalline material adhered to the ITO surface is detected. Higher magnification (Figure 7c) reveals that some of these nanofibers are joined together giving rise to stacks of closely packed nanorods having preferred orientation in which their tips prominently point away from the ITO surface. In contrast, SEM images (Figure 7d) of Mn-TCNQ material obtained at very low scan rate (1 mV s^{-1}), reveal the formation of a compact layer of randomly oriented larger-sized nanorod

(20) Bond, A. M. *Broadening Electrochemical Horizons: Principles and Illustration of Voltammetric and Related Techniques*; Oxford University Press: Oxford, 2002; pp 334−440.

(21) (a) Fletcher, S.; Halliday, C. S.; Gates, D.; Westcott, M.; Lwin, T.; Nelson, G. *J. Electroanal. Chem.* **1983**, *159*, 267. (b) Bond, A. M.; Fletcher, S.; Marken, F.; Shaw, S. J.; Symons, P. G. *J. Chem. Soc., Faraday Trans.* **1996**, *92*, 3925.

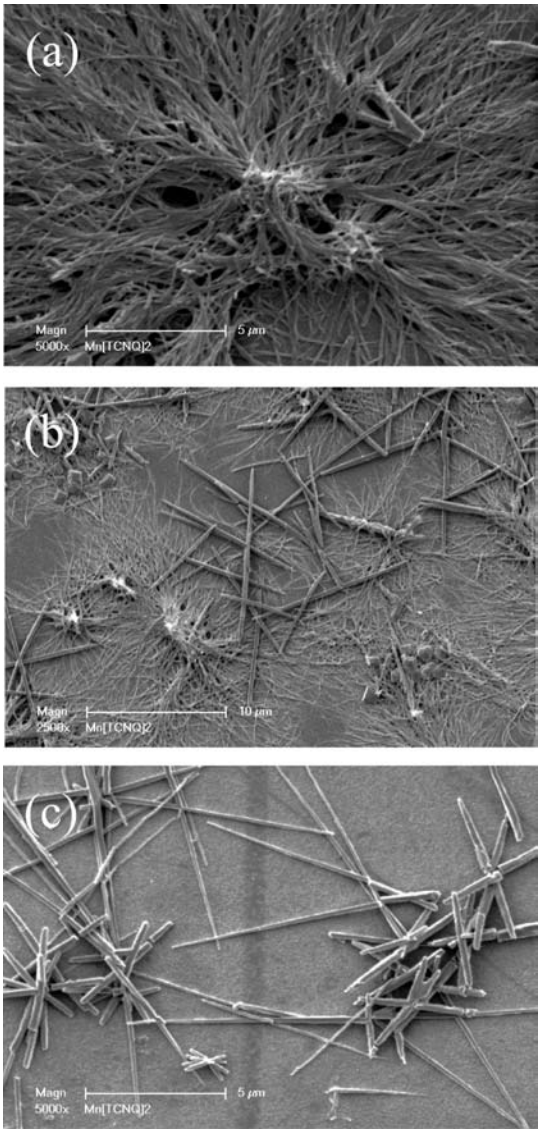

Figure 8. SEM images showing the change in morphology of electrochemically generated Mn-TCNQ material as a result of extensive cycling of the potential over the range of 0.35 to −0.10 V, at a scan rate of 20 mV s^{-1}, when a TCNQ-modified ITO electrode (mechanical attachment) is in contact with 0.10 M $Mn(NO_3)_{2(aq)}$ electrolyte and subjected to 1.5 (image a), 5.5 (image b), and 15.5 (image c) cycles of potential.

structures (lengths 5−10 μm) with an average diameter of about 100−200 nm, consistent with slow crystal growth to give another form of Mn-TCNQ based material.

Interestingly, when an intermediate scan rate (20 mV s^{-1}) is used to induce the transformation process under multicyclic conditions, the relative proportions of both forms of Mn-TCNQ material are determined by the number of cycles. Thus, in the initial stages of this experiment (1.5 cycles), the morphology is again a network of very long and narrow nanofibers (Figure 8a), which mimics that found with faster scan rates or very short electrolysis time. SEM images obtained after 5.5 potential cycles, gives rise to longer (~10 μm) and much thicker nanowire/nanorod structures (Figure 8b), which predominates over the fibrous architecture observed initially. Finally, upon applying 15.5 cycles of the potential, the majority of the electrochemically generated Mn-TCNQ material has a flat and long needle-shaped morphology with crystal dimensions ranging from 5 to 15 μm in length and ~50−100 nm in diameter, consistent with extensive interconversion of the nanofibers into nanorods being achieved under these conditions.

SEM images were also examined to probe the morphology of Mn-TCNQ based material formed via reductive electrolysis. Figure 9 displays an SEM image derived from a region of the surface containing a single ($\approx 50 \times 50\ \mu m^2$) TCNQ microcrystal (image a) immobilized onto an ITO surface via the drop casting method and ones of the electrochemically synthesized Mn-TCNQ based material (images b and c) produced as a result of reductive bulk electrolysis of the crystal at $E_{appl} = -0.10$ V for 10 min, when the TCNQ-modified ITO electrode is placed in contact with aqueous 0.10 M $Mn(NO_3)_2$ solution. Figure 9b (low-magnification image) shows that after 10 min of reductive electrolysis, the parent TCNQ crystal is covered with nanosized needle-like crystals. Higher magnification (Figure 9c) reveals that these nanostructures consist of densely packed, randomly oriented, nanorods having a length of 8−10 μm and a diameter of about 200−300 nm. SEM images (Figure 9d) obtained from a different region of the ITO surface, where smaller-sized TCNQ crystals are initially present, show the formation of relatively short (~2 μm) square-shaped nanorods exhibiting preferred outward growth from the originally small TCNQ crystals.

In accordance with findings associated with the redox-based interconversion of large crystals of solid TCNQ into the analogous $M[TCNQ]_2(H_2O)_2$ (M = Fe, Co, Ni) systems,[16] SEM probing of the TCNQ/Mn-TCNQ transformation at longer (15 min) electrolysis times reveals that all faces (top, edges, and base) of the parent TCNQ crystals are fully covered with a network of densely packed nanowire/nanorod crystals (Figure 10 panels a and b). The nucleation−growth process probably starts at the base of TCNQ crystal[16] where direct contact with the electrode surface and the electrolyte solution occurs presumably at the solid|solid|liquid triple phase junction,[22] namely, in this case, $ITO|TCNQ^{0/\bullet-}{}_{(s)}|Mn^{2+}{}_{(aq)}$ electrolyte. Crystal growth is then progressively extended, owing to the semiconducting nature of the Mn-TCNQ crystals,[11b,12] encompassing the edges as well as the top part of parent TCNQ crystals. Interestingly, when the TCNQ crystals are exposed to an even longer electrolysis time (25 min) the Mn-TCNQ nanosized needle-shaped crystals (Figure 10 panels c and d) exhibited extensive outgrowth, particularly from the central part of the crystal, thereby generating a hollow region and a pattern consisting of nanorod architectures.

A significant conclusion that one can deduce from a combination of voltammetric data and SEM images is that dramatic changes in morphology, crystal size, and packing density of electrochemically generated Mn-TCNQ occurs during the course of voltammetric and controlled potential electrolysis experiments, leading to the observation of time-dependent nanofiber to nanorod morphology conversion. Importantly, careful manipulation of experimental parameters such as scan rate,

(22) (a) Hermes, M.; Scholz, F. *Electrochem. Commun.* **2000**, *2*, 845. (b) Deng, Y.; Wang, D.; Xiao, W.; Jin, X.; Hu, X.; Chen, G. Z. *J. Phys. Chem. B* **2005**, *109*, 14043.

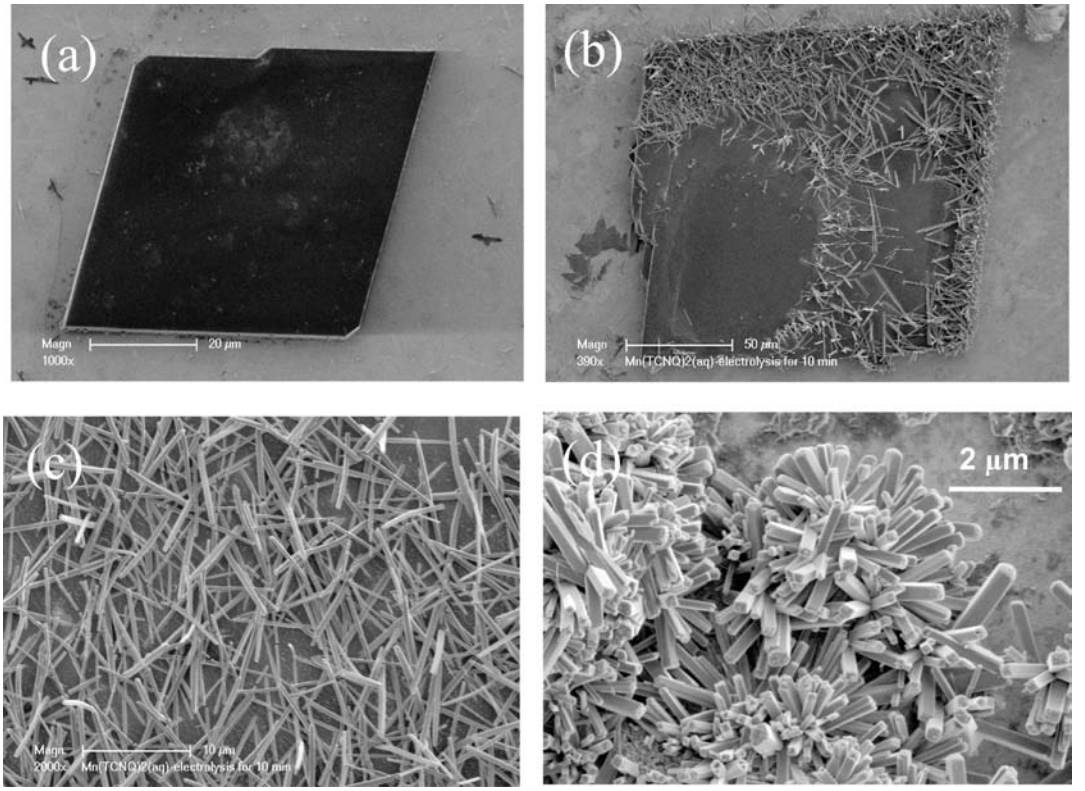

Figure 9. (a) SEM image of a TCNQ-modified ITO electrode prepared via the drop cast method. (b) SEM image presumably showing the formation of the long-term Mn-TCNQ based material on the surface of parent TCNQ crystal upon reductive electrolysis for 10 min at −0.10 V, when the TCNQ-modified ITO electrode is immersed in 0.10 M $Mn(NO_3)_{2(aq)}$ electrolyte. Image (c) shows top-view of image (b), but at higher magnification. Image (d) illustrates Mn-TCNQ nanorods formed under the same conditions but when commencing with smaller-sized TCNQ crystals.

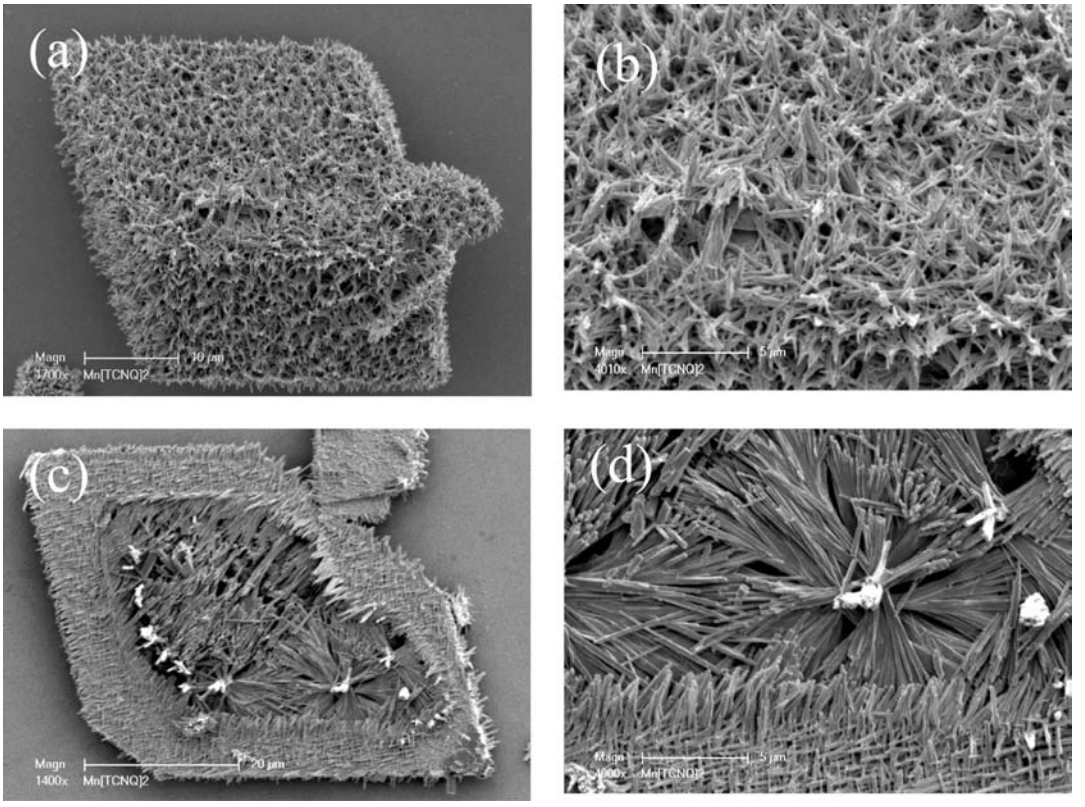

Figure 10. SEM images of Mn-TCNQ material derived by reductive electrolysis at −0.10 V of a large TCNQ crystal present on a TCNQ-modified ITO electrode (drop casting method) in the presence of 0.10 M $Mn(NO_3)_{2(aq)}$ electrolyte at different electrolysis times, (a) 15 min and (c) 25 min. Images (b) and (d) show higher magnifications of images (a) and (c), respectively.

Table 2. Summary of Characteristic Infrared Absorption Bands of Electrochemically-Synthesized $Mn[TCNQ]_2$-Based Materials and Related Compounds

compound	ν(C≡N), (cm^{-1})	ν(C=C), (cm^{-1})	δ(C−H), (cm^{-1})	σ-Dimer	ref
TCNQ	2222 (m)[a]	1542(m)	858 (m)	c	15
$Mn[TCNQ]_2$	2205 (s), 2187 (s), 2137 (sh)	1505 (s)	826 (m)	c	16
$Mn[TCNQ]_2(H_2O)_2$ (bulk)	2211 (s), 2194 (s), 2168 (m)	b	825 (m)	c	17
$Mn[TCNQ]_2(H_2O)_2$ (crystals)	2206 (s), 2197 (s), 2189 (m), 2166 (sh)	b	823 (m)	c	17
$Mn[TCNQ]_2(MeOH)_2$	2214 (s), 2191 (s), 2176 (s), 2159, 2139 (sh)	b	827 (m)	804 (w)	17
$[Mn(TCNQ-TCNQ)(MeOH)_4]_\infty$	2202 (s), 2139 (s)	b	c	806 (m)	17
$[Mn(TCNQ)(TCNQ-TCNQ)_{0.5}(MeOH)_2]_\infty$	2216 (s), 2187 (s), 2168 (m), 2156 (sh)	b	825 (m)	802 (w)	17
$Mn[TCNQ]_2(H_2O)_2$ (chemical synthesis)	2217 (s), 2201 (s), 2175 (m)	1510 (s)	826 (m)	c	d
$Mn[TCNQ]_2(H_2O)_2$ (bulk electrolysis, 1 min)	2212 (s), 2194 (s), 2173 (m)	1508 (s)	824 (m)	c	e
$Mn[TCNQ]_2(H_2O)_2$ (bulk electrolysis, 15 min)	2210 (s), 2196 (s), 2170 (m)	1509 (s)	823 (m)	c	f
$Mn[TCNQ]_2(H_2O)_2$ (cyclic voltammetry, 100 mV/s)	2213 (s), 2192 (s), 2173 (m)	1509 (s)	825 (m)	c	g
$Mn[TCNQ]_2(H_2O)_2$ (cyclic voltammetry, 1 mV s^{-1})	2214 (s), 2194 (s), 2171(m)	1510 (s)	823 (m)	c	h

[a] Relative intensity designations: s = strong, m = medium, w = weak, vw = very weak, sh = shoulder. [b] Not reported. [c] Not observed. [d] Chemically synthesized in our laboratory by reacting aqueous solutions of $Mn(NO_3)_{2(aq)}$ with LiTCNQ as described in Experimental Section. [e] Bulk electrolysis for 1 min at $E_{appl} = -0.1$ V of a TCNQ-modified ITO electrode in contact with 0.1 M aqueous solution of $Mn^{2+}_{(aq)}$ electrolyte. [f] Bulk electrolysis for 15 min at $E_{appl} = -0.1$ V of a TCNQ-modified ITO electrode in contact with 0.1 M aqueous solution of $Mn^{2+}_{(aq)}$ electrolyte. [g] Cyclic voltammetry at a scan rate of 100 mV s^{-1} for 20.5 cycles of the potential over the range 0.35 to −0.1 V using either TCNQ-modified GC or ITO electrodes. [h] Cyclic voltammetry at a scan rate of 1.0 mV s^{-1} for 2.5 cycles of the potential over the range 0.35 to −0.1 V using either TCNQ-modified GC or ITO electrodes.

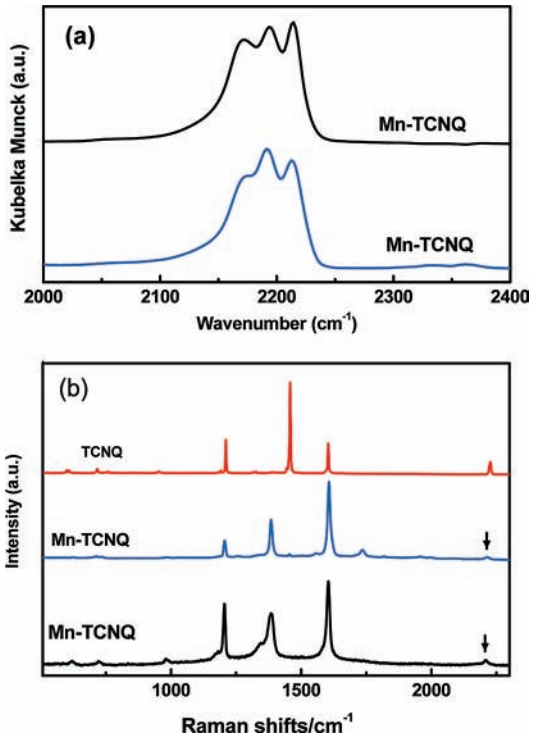

Figure 11. (a) IR spectra in the ν(C≡N) region for Mn-TCNQ based material formed by cyclic voltammetry, 20.5 cycles at scan rate of 100 mV s^{-1} (black trace) and 2.5 cycles at 1 mV s^{-1} (blue trace), over the potential range of 0.35 to −0.10 V with a TCNQ-modified ITO electrode (mechanical attachment method) in the presence of aqueous 0.1 M $Mn(NO_3)_2$ electrolyte. (b) Raman spectra of solid TCNQ and Mn-TCNQ based material formed by reductive electrolysis (15 min) at $E_{appl} = -0.10$ V for a TCNQ-modified ITO electrode (mechanical attachment method) in the presence of aqueous 0.10 M $Mn(NO_3)_2$ electrolyte. The blue and black curves represent the same sample, but from different regions of the electrode surface.

electrolysis time, number of cycles of the potential, and method of electrode modification with solid TCNQ is a crucial factor in controlling the morphology of the electrochemically generated Mn-TCNQ based material.

3.3. Characterization of the Electrochemically Synthesized Mn-TCNQ Based Material. To explore the chemical identity of the stable product(s) generated via reduction processes A^{red} and B^{red}, observed during the redox-based TCNQ/Mn-TCNQ solid−solid interconversion, *ex situ* IR, Raman, X-ray powder diffraction, and EDAX characterization were undertaken.

3.3.1. IR Spectroscopy. Table 2 contains the frequencies (ν) of IR bands observed for electrochemically produced Mn-TCNQ based solids, chemically synthesized $Mn[TCNQ]_2(H_2O)_2$, and literature values for related compounds.[15] *Ex situ* IR spectral features obtained from solid produced by either cyclic voltammetry ($\nu = 100$ mV s^{-1}, 20.5 cycles or $\nu = 1$ mV s^{-1} and 2.5 cycles) or bulk electrolysis for 1 or 15 min at $E_{appl} = -0.10$ V were remarkably similar. Figure 11a illustrates IR spectra in the $\nu_{C\equiv N}$ region obtained under conditions of cyclic voltammetry, while Supporting Information, Figure S3 displays the full range of IR spectra of materials generated via short and long-term bulk electrolysis. In all cases, three well-resolved and intense absorption bands are present at 2213 ± 1, 2193 ± 1, and 2172 ± 1 cm^{-1} in the $\nu_{C\equiv N}$ stretching region. The shifts of the nitrile frequencies, relative to neutral $TCNQ^0$ ($\nu_{C\equiv N} = 2222$ cm^{-1}), are as expected for a $TCNQ^{\bullet-}$ radical anion coordinated to the Mn^{2+} ion.[15,16,23] IR bands in the νC=C stretching region at 1510 ± 1 cm^{-1}, assigned to π-bond delocalization over the TCNQ phenyl ring, also provide supportive evidence for the presence of $TCNQ^{\bullet-}$ in all the electrochemically produced materials.[15,16] In the C−H bending regions, all spectra exhibit sharp δ_{C-H} bending vibrations at 825 ± 2 cm^{-1}, again consistent with coordinated *syn*-μ_2-$TCNQ^{\bullet-}$ ligand.[15,16] Furthermore, the absence of the lower energy C−H stretch ($\delta_{C-H} \sim 806-812$ cm^{-1}), attests to the absence of σ-dimerized $[TCNQ-TCNQ]^{2-}$ dianion[15] in all electrochemically generated materials.

As found with the electrochemically and chemically synthesized $M[TCNQ]_2(H_2O)_2$ (M = Fe, Co, Ni) compounds,[16] the Mn-TCNQ based solids also exhibit broad bands at 3234 and 3367 cm^{-1} that are indicative of the presence of coordinated water [ν_s(OH) and ν_{as}(OH)]. Thus, IR data for all electrochemically synthesized products suggest that they all have the same chemical composition. Furthermore, the excellent agreement between these IR data and those obtained from authentic

(23) Kaim, W.; Moscherosch, M. *Coord. Chem. Rev.* **1994**, *129*, 157.

samples and literature data for $Mn[TCNQ]_2(H_2O)_2$[15] (Table 2), confirms that the electrochemically induced TCNQ/Mn-TCNQ solid−solid transformation gives rise to hydrated $Mn[TCNQ]_2(H_2O)_2$.

Significantly, careful comparison of the IR data obtained for Mn-TCNQ material with those reported for the analogous $M[TCNQ]_2(H_2O)_2$ (M = Fe, Co, Ni)[16] revealed the presence of two IR bands at 1404 and 1290 cm^{-1} in addition to the characteristic C=C wing stretching bands at 1355 and 1330 cm^{-1}. Thus, the full IR spectrum for the Mn-TCNQ material closely compares with those reported for $[Mn(MAC)(TCNQ)_2]$,[24] (MAC = 2,13-dimethyl-3,6,9,12,18-pentaazabicyclo[12.3.1]octadeca-1(18),2,12,14, 16-pentaene), which has been shown via X-ray crystal structures and analysis of electron spin resonance (ESR) data to exhibit strong intermolecular $\pi-\pi$ stacking interactions between the TCNQ radicals (3.2 Å) that lead to interwoven infinite chains.[24] Thus, it is possible on the basis of IR data that $\pi-\pi$ stacking interactions are highly accentuated in the electrochemically generated $Mn[TCNQ]_2(H_2O)_2$ material.

3.3.2. Raman Spectroscopy. Consistent with the IR data, closely related Raman spectra were obtained for Mn-TCNQ-based solids derived electrochemically from TCNQ-modified electrodes in contact with aqueous Mn^{2+} electrolyte solution and those obtained from $Mn[TCNQ]_2(H_2O)_2$ solids prepared chemically[15] or electrochemically via deposition from acetonitrile (vide supra), thereby implying that the phase formed is independent of the preparation method.

Inspection of the representative Raman spectra provided in Figure 11b reveals that the four most intense and characteristic vibration modes of neutral $TCNQ^0$ at 1206 cm^{-1} (C=C−H bending), 1454 cm^{-1} (C=CN wing stretching), 1602 cm^{-1} (C=C ring stretching), and 2225 cm^{-1} (C−N stretching) are influenced by the one-electron reduction to $TCNQ^{\bullet-}$ and its coordination to Mn(II) ions. In particular, the 2225 cm^{-1} band of $TCNQ^0$ (red curve) is shifted by 15 cm^{-1} to lower frequency and its intensity is diminished by formation of Mn-TCNQ solid, as also found in the case of formation of isostructural $M[TCNQ]_2(H_2O)_2$ (M = Fe, Co, Ni) materials.[16] More importantly, the fingerprint vibration mode of $TCNQ^0$ (1454 cm^{-1}) and most sensitive Raman band to $TCNQ^{0/-/2-}$ oxidation states[25] is red-shifted to 1383 cm^{-1} (blue curve in Figure 11b). This significant shift (71 cm^{-1}) in the C=C−N wing stretching matches very well with those found for the congeners $M[TCNQ]_2(H_2O)_2$ (M = Fe, Co, Ni),[16] thereby indicating the presence of coordinated $TCNQ^{\bullet-}$ and hence formation of the $Mn[TCNQ]_2(H_2O)_2$.

Intriguingly, one new feature did emerge in the Raman spectra. Thus, it was noted sometimes the 1383 cm^{-1} band, in the Mn-TCNQ material, is accompanied by a shoulder (black curve in Figure 11b) or even a resolved band (Supporting Information, Figure S4) at 1342 cm^{-1}. This phenomenon is not believed to be a result of a structural change induced by the Raman light source, as repetitive collection of spectra from the same spot did not modify the bands. Although, this new feature has no precedent in the Raman spectra of the isostructural $M[TCNQ]_2(H_2O)_2$ (M = Fe, Co, Ni) compounds,[16] analogous features have been detected in the Raman spectra of systems, such as in [Li-TCNQ][26] and $[Mo^V(dtc)_4](TCNQ)$,[27] (dtc = Me_2NCS_2), that exhibit extensive intermolecular $\pi-\pi$ stacking interactions between the $TCNQ^{\bullet-}$ ligands and hence formation of diamagnetic π-$[(TCNQ)_2]^{2-}$ dimers in the solid state. Moreover, the possible presence of π-$[(TCNQ)_2]^{2-}$ in chemically synthesized $[Mn(TCNQ)_2(H_2O)_2]_\alpha$ polymer also was suggested by Dunbar and co-workers.[15] This suggestion was based on crystallographic evidence which revealed a rather short (~3.1 Å) distance between the $TCNQ^{\bullet-}$ ligands within the *intra*-layers of the extended 2-D polymeric structure, which could exert extensive $\pi-\pi$ stacking interactions that lead to strongly coupled π-dimers at least in some crystals. Thus, the low frequency band at 1342 cm^{-1} in the Raman spectra of the Mn-TCNQ based solids is tentatively attributed to the presence of extensive $\pi-\pi$ interactions of $TCNQ^{\bullet-}$ radicals and formation of π-$[(TCNQ)_2]^{2-}$ in the crystals having the fibrous morphology. The IR data also support this hypothesis. The presence of a σ-$[TCNQ-TCNQ]^{2-}$ dimer or the $TCNQ^{2-}$ radical dianion may be ruled out, since the IR data provide no evidence for $TCNQ^{2-}$[15,23] or the σ-dimerized $[TCNQ-TCNQ]^{2-}$ (~808 cm^{-1}) dianion.

3.3.3. X-ray Powder Diffraction. X-ray diffraction experiments with all electrochemically generated solids give rise to indistinguishable powder patterns. Characteristic diffraction peaks at 14.42°, 16.11°, 19.60°, 23.70°, 25.96°, 33.02°, and 37.46° closely match the literature values reported for chemically synthesized $Mn[TCNQ]_2(H_2O)_2$,[15] thereby confirming the formation of only one crystalline polymorph identified as hydrated $Mn[TCNQ]_2(H_2O)_2$.

3.3.4. Energy Dispersive X-ray. EDAX elemental analysis of all Mn-TCNQ materials generated under a wide range of experimental condition via either reductive electrolysis or cyclic voltammetry revealed the presence of Mn, C, N, and O as expected for formation of the hydrated $Mn[TCNQ]_2(H_2O)_2$ material. The combined spectroscopic and surface science characterization of the electrochemically produced Mn-TCNQ solid confirms the generation of a polymeric material of the hydrated $Mn[TCNQ]_2(H_2O)_2$ that contains $TCNQ^{\bullet-}$ ligands, strongly coupled within *inter*- and *intra*- layers dimers, as found with the chemically synthesized polymer.[15]

4. Discussion

In comparison with the previously reported redox-based $TCNQ/M[TCNQ]_2(H_2O)_2$ (M = Fe, Co, Ni) solid−solid interconversions,[16] it is evident that the manganese system behaves differently to the Fe, Co, and Ni transition metals. In the Mn case, the transformation process occurs via two voltammetrically distinguishable, time-dependent redox processes that lead to generation of $Mn[TCNQ]_2(H_2O)_2$

(24) Madalan, A. M.; Voronkova, V.; Galeev, R.; Korobchenko, L.; Magull, J.; Roesky, H. W.; Andruh, M. *Eur. J. Inorg. Chem.* **2003**, 1995.
(25) Khatkale, M. S.; Devlin, J. P. *J. Chem. Phys.* **1979**, *70*, 1851.
(26) Oohashi, Y.; Sakata, T. *Bull. Chem. Soc. Jpn.* **1973**, *46*, 3330.
(27) (a) Faulques, E.; Leblanc, A.; Molinié, P.; Decoster, M.; Conan, F.; Guerchais, J. E.; Sala Pala, J. *Spectrochim. Acta* **1995**, *51A*, 805. (b) Faulques, E.; Leblanc, A.; Molinié, P.; Decoster, M.; Conan, F.; Sala Pala, J. *J. Phys. Chem. B* **1997**, *101*, 1561.

material exhibiting nanofiber or nanorod network morphologies.

The voltammetric behavior of the Mn system while not seen with other divalent transition metal systems, finds analogy in the study of Chambers et al.[28] on TCNQ-polyester polymer films modified electrodes in acetonitrile and aqueous media containing alkali metal electrolytes. In that study, the initial voltammetric reduction is assigned, on the basis of ESR and UV−visible evidence, to facile formation of a "mixed-valence" anion dimer radical, $[TCNQ-TCNQ]^{\bullet -}$, via radical-substrate coupling reaction between $TCNQ^{\bullet -}$ and $TCNQ^0$, where the unpaired electron is delocalized over the two TCNQ units. The $[TCNQ-TCNQ]^{\bullet -}$ is then further reduced at a slightly more negative potential (~45 mV) to the dimer dianion, $[(TCNQ)_2]^{2-}$ or disproportionates to regenerate neutral TCNQ and $TCNQ^{\bullet -}$ radical as illustrated by eqs 1−3.

$$TCNQ + e^- \rightleftharpoons TCNQ^- \quad (1)$$

$$TCNQ + TCNQ^- \underset{\text{disp}}{\overset{\text{dim}}{\rightleftharpoons}} [(TCNQ - TCNQ]^{\cdot -} \quad (2)$$

$$[(TCNQ - TCNQ]^{\cdot -} + e^- \rightleftharpoons [(TCNQ)_2]^{2-} \quad (3)$$

as that found when $Mn[TCNQ]_2(H_2O)_2$ material is formed at short time scales. The second pathway, leading to formation of nanorods of $Mn[TCNQ]_2(H_2O)_2$, which is dominant at long time scales (very slow scan rates) is then postulated to take place via a disproportionation mechanism as shown by eq 6 (Scheme 1). Different kinetics may apply in the solid−solid phase interconversion of the analogous TCNQ/$M[TCNQ]_2(H_2O)_2$ (M = Fe, Co, Ni) systems[16] and gives rise to conditions needed to form long and thick nanorods.

In contrast to the complexity associated with two pathways for the formation of $Mn[TCNQ]_2(H_2O)_2$ via reduction of TCNQ in a solid−solid transformation, the oxidation processes (C^{ox} and D^{ox}) appear to be more straightforward, and in the overall sense may be represented by eqs 7 and 8.

$$GC|\{Mn[TCNQ]_2(H_2O)_2\}_{(\text{nanofibers})} \xrightarrow[C^{ox}]{-2e^-} Mn^{2+}{}_{(aq)} + 2TCNQ_{(s,\,GC)} + 2H_2O \quad (7)$$

$$GC|\{Mn[TCNQ]_2(H_2O)_2\}_{(\text{nanorods})} \xrightarrow[D^{ox}]{-2e^-} Mn^{2+}{}_{(aq)} + 2TCNQ_{(s,\,GC)} + 2H_2O \quad (8)$$

The difference in potential (~100 mV) for oxidation processes C^{ox} and D^{ox} is attributed to marked differences

Scheme 1

$$4\,TCNQ_{(\text{solid, GC})} + Mn^{2+}{}_{(aq)} + 2e^- \rightleftharpoons [(Mn^{2+})(TCNQ\text{-}TNQ)_2^{\bullet -})]_{(\text{solid, GC})} \quad (4)$$

$$[(Mn^{2+})(TCNQ\text{-}TNQ)_2^{\bullet -})]_{(\text{solid, GC})} + Mn^{2+}{}_{(aq)} + 2e^- \overset{2\,H_2O}{\rightleftharpoons} 2\{Mn[TCNQ]_2(H_2O)_2\}_{(\text{nanofibers, GC})} \quad (5)$$

Disp

$$2\,TCNQ_{(\text{solid, GC})} + \{Mn[TCNQ]_2(H_2O)_2\}_{(\text{nanorods, GC})} \quad (6)$$

The combined voltammetric, spectroscopic, and microscopic findings in this study emphasize that time plays a crucial role in controlling the morphology of the electrochemically synthesized $Mn[TCNQ]_2(H_2O)_2$ material. Thus, under conditions of fast scan rate or very short electrolysis time scales, electrochemical generation of $Mn[TCNQ]_2(H_2O)_2$ (first route) is assumed to occur rapidly via incorporation of $Mn^{2+}{}_{(aq)}$ ions, from bulk solution, into the mixed valence anion dimer, $[TCNQ-TCNQ]^{\bullet -}$, formed via charge-transfer reaction between initially generated $TCNQ^{\bullet -}$ and solid $TCNQ^0$, giving rise to a Mn-stabilized TCNQ anionic dimer, $[(Mn^{2+})(TCNQ-TCNQ)_2^{\bullet -}]$, which is then further reduced at a slightly more negative potential to give $Mn[TCNQ]_2(H_2O)_2$ as described in eqs 4 and 5 in Scheme 1.

In the electrocrystallization of structurally analogous $Co[TCNQ]_2(H_2O)_2$ onto an electrode surface by reduction of TCNQ in the presence of Co^{2+} in acetonitrile, reduction of a similar Co stabilized dimer anion, $[(Co^{2+})(TCNQ-TCNQ)^{\bullet -}{}_2]$, was suggested as a possible route for electrodeposition of crystalline thin films of the isolated $Co[TCNQ]_2(H_2O)_2$ material.[10b] This pathway generated the same morphology of a compact network of nanofibers in crystal size, packing arrangements and density, and morphology of the $Mn[TCNQ]_2(H_2O)_2$ material. Thus, egress of the $Mn^{2+}{}_{(aq)}$ that accompanies oxidation of small nanofiber crystals via process C^{ox} is kinetically more facile (less overpotential) than its egress from larger nanorods that occurs in process D^{ox}.

5. Conclusions

In contrast to the single step TCNQ/$M[TCNQ]_2(H_2O)_2$ (M = Fe^{2+}, Co^{2+}, Ni^{2+}) solid−solid transformation processes detected at a TCNQ modified electrode in contact with aqueous M^{2+} electrolytes, the electrochemically induced solid−solid phase transformation of microcrystalline TCNQ into Mn-TCNQ material occurs through two voltammetrically distinct, time dependent, processes that generate fibrous and nanorod forms of $Mn[TCNQ]_2(H_2O)_2$ solid. The initial step is assumed to involve incorporation of $Mn^{2+}{}_{(aq)}$ ions into $TCNQ^{\bullet -}$ crystal lattice at the $GC|TCNQ^{0/\bullet -}|Mn^{2+}{}_{(aq)}$ triple phase junction following a nucleation/growth mechanism. Precise control of experimental parameters such as scan rate, electrolysis time, $Mn^{2+}{}_{(aq)}$ concentration, and the method of electrode modification are postulated to facilitate generation of $Mn[TCNQ]_2(H_2O)_2$ via either a rapid and direct electron transfer pathway or a slower one that includes disproportionation of the Mn-stabilized intermediate.

(28) (a) Gyorgy Inzelt, G.; Day, R. W.; Klnstle, J. F.; Chambers, J. O. *J. Phys. Chem.* **1983**, *87*, 4592. (b) Karimi, H.; Chambers, J. O. *J. Electroanal. Chem.* **1987**, *217*, 313.

SEM images reveal that $Mn[TCNQ]_2(H_2O)_2$ produced by the two electrochemical pathways have different morphologies (nanofiber versus nanorod). However, analysis of IR, Raman, EDAX, and X-ray diffraction data implies that the two forms have the same chemical composition and represent only one crystalline phase of hydrated $Mn[TCNQ]_2(H_2O)_2$ solid. On this basis, the difference in peak potentials for oxidation of the two forms, manifested by a separation of ~100 mV in processes C^{ox} and D^{ox}, is attributed to differences in morphology (nanofiber versus rod-like) of the $Mn[TCNQ]_2(H_2O)_2$ material and hence in kinetics associated with rate of egress of $Mn^{2+}_{(aq)}$ from the $TCNQ^{\bullet-}$ lattice. On the basis of these findings, direct and rapid electrochemical generation of the $Mn[TCNQ]_2(H_2O)_2$ is assumed to take place via radical-substrate coupling of $TCNQ^{\bullet-}$ and neutral TCNQ accompanied by ingress of Mn^{2+} ions from the aqueous electrolyte to form a Mn-stabilized intermediate, $[(Mn^{2+})(TCNQ-TCNQ)_2^{\bullet-}]$, which undergoes further reduction at a more negative potential to form a polymeric $Mn[TCNQ]_2(H_2O)_2$ material as a nanofiber network. On the other hand, formation of the nanorods of $Mn[TCNQ]_2(H_2O)_2$ form may be assisted by slow disproportionation of the initially formed intermediate, followed by regeneration of neutral TCNQ, which is involved again in the reduction process.

Voltammetric findings suggest that differences of the electrochemically induced $TCNQ/Mn[TCNQ]_2(H_2O)_2$ solid−solid interconversion compared to other $TCNQ/M[TCNQ]_2(H_2O)_2$ (M = Fe, Co, Ni) family members of the divalent transition metal may arise from kinetically controlled accessibility of two time-resolved routes for its formation. Importantly, this allows tuning of the morphology of the electrochemically generated $Mn[TCNQ]_2(H_2O)_2$ material.

Acknowledgment. We gratefully acknowledge the Australian Research Council for financial support of this work and also thank Dr Lisandra Martin (Monash University) for useful discussions and Dr Alexander Bylik and Steven Pentinakis from the CSIRO Division of Manufacturing and Materials (CMMT) for technical assistance with the SEM and EDAX measurements.

Supporting Information Available: Figures showing (Figure S1) cyclic voltammograms as a function of the number of cycles of potential with a TCNQ-modified ITO electrode, (Figure S2) voltammetric behavior of electrocrystallized $Mn[TCNQ](H_2O)_2$, (Figure S3) IR, and (Figure S4) Raman spectra of Mn-TCNQ based solids formed by bulk electrolysis. This material is available free of charge via the Internet at http://pubs.acs.org.